Experimental observation and numerical simulation of transient "stress fangs" within flowing molten polyethylene

K. Lee and M. R. Mackley[a)]

Department of Chemical Engineering, University of Cambridge, Pembroke Street, Cambridge, CB2 3RA United Kingdom

T. C. B. McLeish and T. M. Nicholson

IRC in Polymer Science and Technology, Department of Physics and Astronomy, University of Leeds, Leeds, LS2 9JT United Kingdom

O. G. Harlen

Department of Applied Mathematics, University of Leeds, Leeds, LS2 9JT United Kingdom

(Received 6 December 2000; final revision received 22 May 2001)

Synopsis

We report experimental observations and matching numerical simulation for the time-dependent start-up flow of two molten polyethylenes (PEs) within a slit entry and exit geometry. For the case of a low density polyethylene (LDPE), an unexpected transient, birefringence ''stress fang'' was observed downstream of the slit exit. The stress fang consisted of a localized region of stress concentration. The stress fang, however, was not observed for a linear low density polyethylene (LLDPE) sample subjected to the same processing condition. A matching time-dependent numerical simulation of the flow is also presented. Using a split Lagrangian–Eulerian method for simulating transient viscoelastic flow with the multimode pom–pom constitutive equation, the general features of the stress fangs were predicted for the LDPE. In addition, the simulation did not predict stress fangs for the LLDPE. The paper demonstrates that for this particular case the pom–pom model can successfully discriminate the complex flow behavior of different PEs, and shows that the presence (or otherwise) of a stress fang is sensitive to the particular rheology of the polymer that arises from long chain branching. © *2001 The Society of Rheology.* [DOI: 10.1122/1.1389316]

I. INTRODUCTION

The matching of polymer processing flows to numerical simulation has been reported by a number of authors where, for example, they compare features such as the overall pressure drop, die swell ratio, stress birefringence, and velocity field with a numerical simulation that has matching boundary conditions [see for example, Kiriakidis *et al.* (1993), Koopmans (1992), Ahmed *et al.* (1995), Baaijens *et al.* (1997)]. In particular, in the past, the entry and exit flow through a sudden contraction with a downstream

[a)]Author to whom all correspondence should be addressed. Electronic mail: mrm1@cheng.cam.ac.uk

© 2001 by The Society of Rheology, Inc.

exit of a free surface or a channel has been commonly studied [see, review by Boger *et al.* (1992)]. This benchmark flow mimics many aspects of real processing situations (such as, die entry during injection molding), where areas of combined shear and extensional flow exist. Combined experimental/numerical studies of the complex flow in several other geometries have also been performed [see for example, review by Baaijens *et al.* (2000)].

In recent years, the numerical simulation of the complex viscoelastic behavior of polymer melts has progressed considerably with the development of more reliable numerical schemes and constitutive equations [see for example, Baaijens (1998)]. In terms of constitutive equations that model polymer melt rheology, the K-B.K.Z. [Bernstein *et al.* (1963), Wagner and Laun (1978)], Phan-Thien Tanner [Phan-Thien Tanner (1977), Phan-Thien (1978), Tanner (1979)], and more recently, the ''pom–pom'' [McLeish and Larson (1998)] class of models designed to model long chain branched melts, are among the most robust viscoelastic constitutive equation tested. However, in the past, numerical simulations using these models, have in general, been for steady state, isothermal and two-dimensional flow.

An experimental technique for generating precise, time dependent, repeatable results under accurately controlled flow conditions is now available using the multipass rheometer (MPR). The MPR has been under development in Cambridge for the last five years [Mackley *et al.* (1995), Mackley and Spittler (1996)]. This advanced form of a twin-piston, controlled speed rheometer is capable of accessing processing performance, including the facility to perform flow birefringence observations and in particular, time-dependent flow measurements using small quantities of material [Ranganathan *et al.* (1999), Lee and Mackley (2000)].

This paper reports the time-dependant experimental flow birefringence data that has been obtained using a multipass rheometer and matches this data with a time-dependent numerical simulation that uses a multimode extension of the pom–pom model, which in turn has been implemented into a numerical scheme.

II. RHEOLOGICAL MODEL AND CHARACTERIZATION

A. The pom–pom constitutive model

This new class of constitutive equation was developed by McLeish and Larson [McLeish and Larson (1998)] and is based on the tube theory for an idealized branched molecular geometry having two identical q-armed stars connected by a ''cross-bar segment.'' A key feature is the separation of time constants for cross-bar *stretch* relaxation (τ_s) and cross-bar *orientation* relaxation (τ_b). An individual pom–pom is thus characterized by two relaxation times, the number of arms (q_i) that corresponds to the maximum stretch possible and a modulus (G_i).

In a multimode extension of the pom–pom equations [Inkson *et al.* (1999)], the polymer is modeled as a spectrum of up to 12 pom–pom modes, each mode with differing constitutive parameters. For a highly branched polymer, the slower modes with higher numbers of arms, q, can be thought of as modeling the inside portions of the molecules, constrained by many branch points; whilst the faster modes, with lower q, model the more easily relaxed ends of the molecule (Fig. 1). This *decoupling* of the different levels of branching on a molecule is justified in that the modes with relaxation times much shorter than the time scale of a particular flow will remain relaxed; whilst longer relaxation time (slower) modes will tend to be fully extended and do not relax significantly. At a particular strain rate, only a few modes will be active and thus *coupling* between them

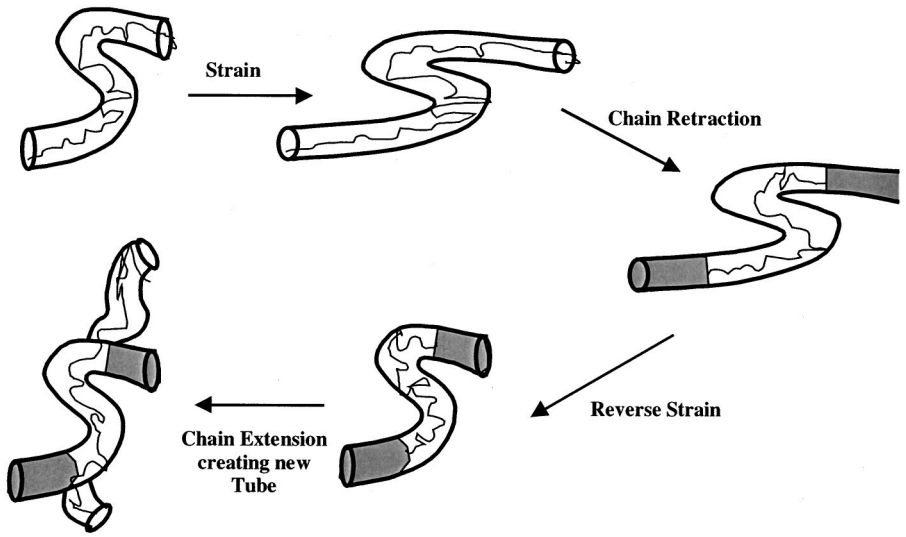

FIG. 1. Schematic illustration of the mechanism by which rapidly reversing flows generate new isotropic tube segments. The formation rate of the new segments at the tube extremities is described by the new term in Eq. (2).

will be expected to be small. This is partially supported by a recent paper by Blackwell *et al.* (2001) comparing the multimode pom–pom model with a rigorous calculation of the dynamics of a Cayley tree molecule. Although this paper identifies a high-strain phenomenon that arises from coupling between modes, it remains perturbative for moderate strains.

In this paper, we highlight mainly the improvements/modifications of the existing pom–pom model necessary to treat our strong reversing flow. Further description of the pom–pom constitutive equation in relation to this paper can be found in [Bishko *et al.* (1999)].

1. Branchpoint withdrawal

Several new additions to the pom–pom model have been incorporated into the simulation program used in this paper. First, the problem of what happens as the maximum stretch for a mode is reached is considered by introducing a *drag strain coupling* term between the relaxed and unrelaxed polymer segments at the branch points, thus modifying the equation that updates the cross-bar stretch (λ) [Blackwell *et al.* (2000)] to become

$$\frac{D\lambda}{Dt} = \lambda(\mathbf{S}:\mathbf{K}) - \frac{1}{\tau_s}(\lambda - 1)e^{\nu^*(\lambda-1)} \quad \text{for } \lambda < q. \tag{1}$$

Here, the first term gives the effect of the material deformation on the stretch, where **K** is the applied strain tensor, **S** the pom–pom cross-bar orientation tensor and (**S:K**) the component of the strain acting along the cross-bar tube. The second term gives the relaxation of the pom–pom cross-bar stretch, where τ_s is its relaxation time. The exponential term models the drag strain coupling with ν^* a new parameter whose best value has been found to be $2/q$ [Blackwell *et al.* (2000)]. This modifies the stretch relaxation time to account for local motion of the branch point and has been shown to give a smoother fit to the experimentally observed rheological behavior. The parameters shown

TABLE I. Relaxation times spectrum and the corresponding non-linear constitutive parameters of the pom–pom model for the LLDPE DOWLEX™ and LDPE LD150 melt at 190 °C.

LLDPE DOWLEX™				
Mode No.	τ_b /(s)	Ratio ($\tau_b:\tau_s$)	G_i /(Pa)	Arms (q)
1	0.0025	2	1.45×10^5	1
2	0.0114	2	98 900	1
3	0.0516	2	37 700	1
4	0.235	2	7480	2
5	1.07	2	1400	4
6	4.84	2	152	5
7	22.0	2	18.6	22
8	100	0.5	0.162	165
LDPE LD150				
Mode No.	τ_b /(s)	Ratio ($\tau_b:\tau_s$)	G_i /(Pa)	Arms (q)
1	0.00 312	2	1.55×10^5	1
2	0.0260	2	75 400	1
3	0.216	2	42 200	1
4	1.80	2	19 600	1
5	15.0	2	7530	4
6	125	2	1870	4
7	1040	2	189	9
8	8670	2	14.1	10
9	72 200	2	2.05	14
10	602 000	2	0.340	16

in Table I (Sec. II B) have been fitted including this term. As in the original model, the stretch, λ, is constrained to be no more than the number of free arms attached to the branch point, q. Once the stretch reaches this limit the arms are withdrawn into the tube. However, since the contribution from the withdrawn arms is small, we do not need to calculate amount of arm withdrawal [McLeish and Larson (1998), Inkson *et al.* (1999)].

2. Decelerating or reversing flows

A second important modification to the pom–pom equations that we introduce here considers ''decelerating flows,'' in which the tube may be retracting faster than the chain. This may occur in ''reversing flows'' when a forward strain is followed by a strain of opposite sign, such as in the constriction geometry studied in this work; extrudate swell would be another example. If the reversal is immediate, then the strain follows almost affinely. However, if there has been significant chain retraction in the intervening period or if the segments are extended to their maximum length during the forward strain, then the contraction of the tube length during the reversing strain may bring the primitive path *below* its equilibrium length, so that $\lambda < 1$. From the stretch-equation (1), it is easy to show that this condition is equivalent to $(\mathbf{S}:\mathbf{K}-\dot{\lambda}/\lambda) < 0$, (where $\dot{\lambda} \equiv D\lambda/Dt$) meaning that the tube is being forced by the flow to reduce its contour length faster than the chain can retract with it. In this case, new isotropic portions of tube will be formed by chain extension at the tube extremities (at a rate $\mathbf{S}:\mathbf{K}-\dot{\lambda}/\lambda$) in addition to reptation (at a rate $\tau_b{}^{-1}$). The process is illustrated on the molecular level in Fig. (1), in which a typical molecule and its associated tube is followed through a large reversing deformation. On the rapid reversing deformation, new tube segments are created at the rate of the revers-

ing strain, rather than at the natural cross-bar reptation rate. The original pom–pom equations do not capture this process, so the equation for the cross-bar tube orientation needs to be modified to account for it. In this work we treat it at the simplest possible level by modifying the orientation relaxation rate to

$$\frac{1}{\tau_b^*} = \begin{cases} \dfrac{1}{\tau_b} & \text{for } 1 \leqslant \lambda \leqslant q \\ \dfrac{1}{\tau_b} + \dfrac{\dot{\lambda}}{\lambda} - \mathbf{K}:\mathbf{S} & \text{for } \lambda < 1 \end{cases} . \tag{2}$$

This modification of the orientation relaxation time is incorporated into the differential version of the pom–pom orientation equation, where the orientation of a pom–pom element is stored internally in the constitutive model in a tensor **A** that is related to the actual orientation tensor **S** by

$$\mathbf{S} = \frac{\mathbf{A}}{\text{trace}\,(\mathbf{A})}. \tag{3}$$

This tensor **A** satisfies an Oldroyd equation

$$\overset{\nabla}{\mathbf{A}} = -\frac{1}{\tau_b^*}(\mathbf{A}-\mathbf{I}). \tag{4}$$

A similar nonanalytic structure was used by Wagner and Ehricke (1998) to improve the fit of integral constitutive models to data from reversing flows of polymer melts. A more sophisticated tube-model treatment of the mechanism treated here was made in the case of monodisperse linear polymers by Doi [Doi and Edwards 1996]. It accounted well for data on a well-characterized entangled solution of linear polymers [Osaki *et al.* (1981)].

B. Fitting the model parameters: G_i, τ_b, τ_s, q

The stress in the multimode pom–pom model is given by

$$\boldsymbol{\sigma} = 3\sum_i G_i \lambda_i^2 \mathbf{S}_i ,$$

where for each mode i, there is a separate equation for the stretch and orientation given by Eqs. (1)–(4). Thus, there are four material dependent parameters required for each mode. First, the linear relaxation spectrum of the material was determined from the simple shear, linear dynamic moduli measurements using a Rheometrics dynamic spectrometer RDSII [see, for example, Mackley *et al.* (1994)]. This determines the moduli G_i and cross-bar orientation times (τ_{bi}) as a spectrum of moduli (G_i) for corresponding time constants. Each mode of the linear spectrum is then assigned two further parameters, stretch relaxation (τ_{si}), and number of arms (q_i), which are obtained by fitting data from transient uniaxial extensional performed on a Rheometrics RME extensional rheometer. For each extensional experiment, only one or two modes will be active, therefore, the data fitting is not as arduous as might first be thought. This formulation produces a set of parameters that has been shown to model *simultaneously* shear, uniaxial and planar extensional data [Inkson *et al.* (1999)].

Figure 2 shows the fit to the rheological data and Table I the resulting parameters obtained for the two polymers under consideration. It is interesting to note that the fit for

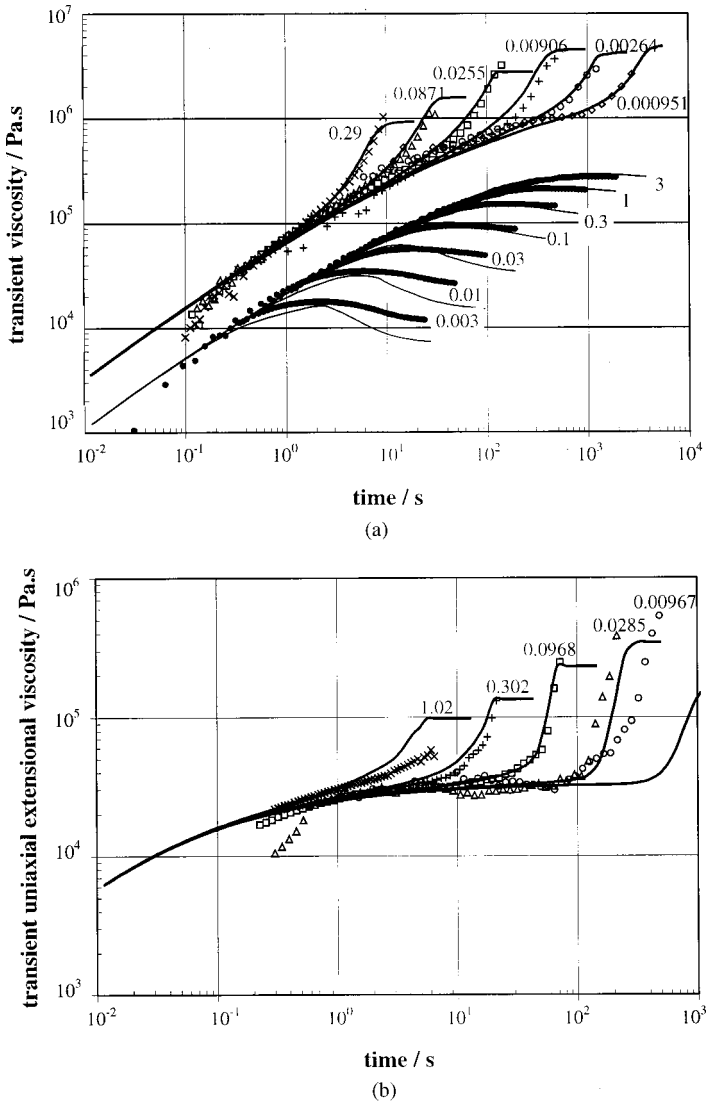

FIG. 2. Fitting of the pom–pom parameters (τ_s, q) from the viscometric data of (a) LDPE LD150 (upper plots are extensional data, lower plots are shear data) and (b) LLDPE DOWLEX (extensional data only), for the given sets of linear spectrum (G_i, τ_b) as listed in Table I. The label of each curve denotes the constant effective strain rate at which the transient experiments were carried out.

the low density polyethylene (LDPE) (a long-chain branched polymer) is better than that for the linear low density polyethylene (LLDPE) (a blend of linear and short-chain branched polymer), which is to be expected since the pom–pom constitutive equation was constructed to model *branched* polymers. Nevertheless, there is some degree of agreement for the LLDPE, which suggests that the *decoupling* of orientation and stretch degrees of freedom are in general true for all *entangled* polymers. This conclusion is also supported by tube models for both linear and branched polymers. The meaning of the q parameters in the context of linear polymers is less immediately clear at a molecular level than for branched, but in both cases control the diminishing of extension hardening at high strains.

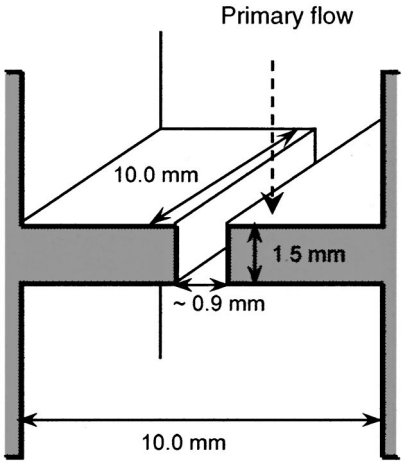

FIG. 3. A schematic of MPR slit inserts with length of 1.5 mm (primary flow direction), width of approximately 1.0 mm (shear gradient direction), and depth of 10.0 mm (neutral direction). The upstream and downstream flow channels are square cross section (10 mm×10 mm).

III. COMPLEX FLOW IN A MPR

Two commercial polyethylene melts of Dow Chemicals were tested: a conventional Ziegler–Natta based LLDPE (Dowlex™ NG5056E) and a LDPE (LD150R, Lot MJ-237081321). The polyethylenes (PEs) were characterized at 190 °C, as described in Sec. II B.

Planar entry and exit flow through a slit geometry was carried out with the PE melts in a MPR fitted with stainless steel slit die inserts. A schematic of the slit flow region, which was integrated with the optical system in a MPR for flow birefringence observations is shown in Fig. 3. Details of the optical setup can be found in [Lee and Mackley (2000)]. The experimental stress field was mapped from the birefringence patterns, assuming that the linear stress optical rule is valid for the PEs studied. Flow-induced birefringence is an optical characteristic exhibited by a molten polymer when it becomes anisotropic by the effect of orientation during flow [see for example, Wales (1976)]. The level of anisotropy can be quantified according to the linear stress optical rule [Eq. (5)] in terms of the principal stress difference (PSD). Therefore, the experimental PSD can be computed from the flow birefringence patterns by counting the relative retardation (or fringe order), k, $= 0, 1, 2, 3...$ and using a value of the stress optical coefficient, $C = 1.74\times10^{-9}\ \mathrm{Pa}^{-1}$, as used and validated for polyethylene by amongst others Lee and Mackley (2000).

$$\Delta n = C(\Delta \sigma), \tag{5}$$

where Δn is the birefringence, which can be measured experimentally as Eq. (6):

$$\Delta n = \frac{k\nu}{d}, \tag{6}$$

where ν is the wavelength of monochromatic light, which in this case was 0.514 nm, and d the depth of sample through which the light propagates (in the neutral direction), which in this case was 10 mm. This equation assumes the material is homogeneous, having constant optical properties along the direction of light propagation. Birefringence is an

integrated effect along a light beam and Eq. (6) is only strictly true for a genuine two-dimensional flow, consequently there will be errors due to end effects near the boundaries. For three-dimensional flows, a more complex approach is required [Baaijens (1994)].

IV. NUMERICAL SIMULATIONS

The time-dependent flow of polymer in the multipass rheometer was simulated using the Lagrangian–Eulerian finite element solver developed at Leeds University [Harlen *et al.* (1995), Bishko *et al.* (1999)], using the pom–pom constitutive model described in Sec. II A. In this method the fluid velocity at each time step is calculated using a standard *Eulerian* finite element technique, while the evolution of the stress is calculated in a *Lagrangian* frame by allowing each element to deform with the local velocity gradient. Details of the numerical method are given in Harlen *et al.* (1995), and Bishko *et al.* (1999).

The flow domain is divided into triangular elements, with velocities and pressures held at the vertices in a continuous interpolation, and material constitutive parameters (cross-bar orientation and stretch) piecewise constant on each element. Modes with relaxation rates much faster than the fluid velocity gradients behave as a Newtonian fluid with viscosity $G_i\tau_{bi}$, and so to reduce computational time, modes for which $\dot{\gamma}\tau_{bi} \leqslant 0.01$ were treated as Newtonian solvent. Here $\dot{\gamma} = Q/d^2$ is the typical shear rate in the constriction where Q is the area flow rate and d is the width of the channel.

At each time-step the velocity ($\mathbf{u}$) and pressure (p) are found from a finite element solution of the equations of mass and momentum conservation

$$\mu\nabla^2\mathbf{u} - \nabla p = -\nabla\boldsymbol{\sigma}, \tag{7}$$

$$\nabla\cdot\mathbf{u} = 0. \tag{8}$$

Here μ is the effective viscosity formed from the short relaxation time modes. The calculated velocities are then used to advect the grid with the flow and the corresponding triangle deformations are used to update the internal constitutive parameters for the triangles, by solving Eqs. (1) and (4) in the frame that is deforming with the fluid [see Harlen *et al.* (1995)]. The vertices are then reconnected as necessary to maintain a *Delaunay* triangulation. The reconnection process introduces a small degree of stress diffusion. The resolution of the grid is maintained by an automated adaptive routine which divides any element whose side length is greater than a prescribed maximum length, $l_{\max}$ (which is a function of position, so that finer grids may be specified in regions of high gradients).

At the start of the simulation the entire domain is filled with undeformed fluid. Since the flow domain is symmetric only half of the domain needs to be calculated. In order to reduce the size of the calculation further, a full two-dimensional (2D) model is only employed in the region from two channel widths upstream to two channel widths downstream of the contraction. (the simulation domain with mesh refinement is shown in Fig. 5). The region far upstream of the contraction is modeled as a start-up flow in a uniform channel using a one-dimensional simulation employing the same pom–pom constitutive equations. These velocities are then transferred to vertices in the flow entry region of the 2D simulation. Observation of the results indicates that deviations from uniform channel flow do not start until well into the modeled region. Thus, any upstream effects of the piston in the experimental geometry are not modeled. At the bottom of the simulated

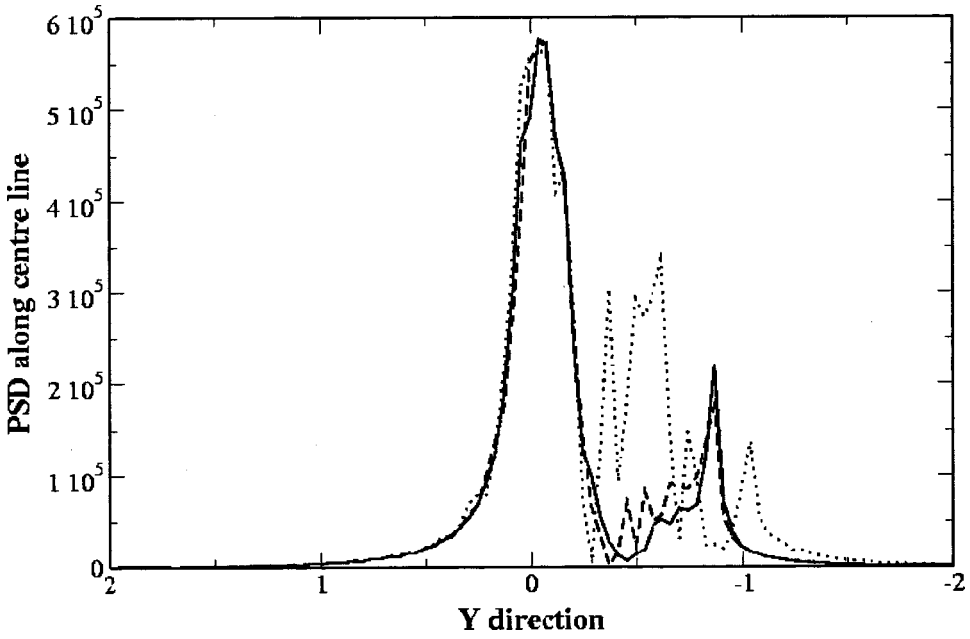

FIG. 4. Centerline stresses calculated for three levels of mesh refinement, indicating convergence of the simulations. All subsequent simulation results presented use the highest level of refinement.

region, vertices are removed from the simulation and velocities from the uniform one-dimensional channel flow model are imposed on the flow exit boundary points.

The presence of the sharp right-angled corners at the entrance to the contraction produces a stress singularity, which causes problems in numerical simulations. However, unlike the Oldroyd B model [investigated by Davies and Devlin (1993), Hinch (1993), and Renardy (1993)] the stress in each pom–pom mode cannot exceed $G_i q_i^2$ and so the singularity is no worse than that encountered for a Newtonian fluid. Following the work of Bishko *et al.* the corners in the simulations were rounded with a radius of 1% of the channel radius to avoid the singularity. This limitation of the stress at high deformation rates means that the pom–pom model does not suffer from the numerical problems at a high Weissenberg number that are experienced with other viscoelastic models.

In order to test the convergence of the numerical scheme three different levels of mesh refinement were used in the region near the contraction. The coarse, medium, and fine meshes on average contain 3000, 6000, and 11 000 elements, respectively. The medium mesh at the beginning of the simulation is illustrated in Fig. 5. In the fine mesh there are approximately ten elements spanning the narrow constriction in the center of the simulation. The axial component of stress along the symmetry axis from simulations at the three levels of mesh refinement is compared in Fig. 4, showing that the stress is converging with grid refinement. The results in the remainder of this paper are from the finest mesh. Each simulation took approximately 50 h to run on a 633 MHz Pentium III processor, the run time scaling as the square of the number of elements.

V. THE MATCHING OF EXPERIMENTAL OBSERVATION AND SIMULATION RESULTS

The overall (entry and exit) flow birefringence observations of DOWLEX and LD150 melts during the start-up of flow through a planar geometry of the type shown in Fig. 3

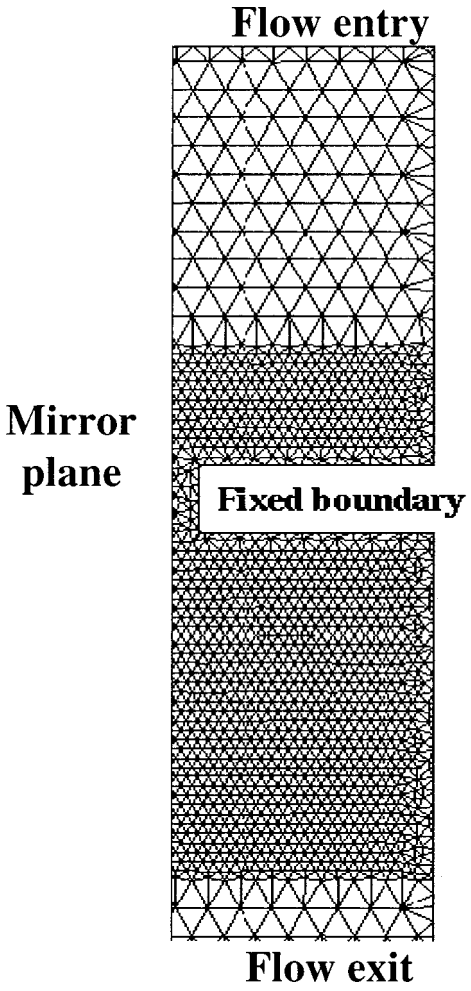

FIG. 5. Finite element simulation mesh of triangular elements at the start of the simulation.

for the MPR are compared to values of $\Delta\sigma$ obtained from the simulations. The principle stress difference $\Delta\sigma$ is directly proportional to the birefringence through the stress optical law, Eq. (5). It is important to note that the simulations assume that the flow is two-dimensional while the experiments have three-dimensional components. The polymer deformation giving rise to the birefringence pattern and pressure drop emanate from the large velocity gradients in and near the contraction, so that in this region the effective aspect ratio in the experiment is 10–1. Consequently the flow along the center plane will be approximately two-dimensional.

In this paper, we consider only one flow condition: volumetric flow rate of $11.3\,\mathrm{mm^3\,s^{-1}}$ (piston speed of $0.1\,\mathrm{mm\,s^{-1}}$) at a temperature of 190 °C. In the simulations this corresponds to an area flow rate of $1.13\,\mathrm{mm^2\,s^{-1}}$. In experiments reported here, the multipass rheometer was operated in a single shot mode, where the two pistons started from rest and were then moved together in the same direction at a constant speed. The simulations were carried out for transient, two-dimensional, and isothermal flow conditions using the pom–pom model with the constitutive parameters given in Table I.

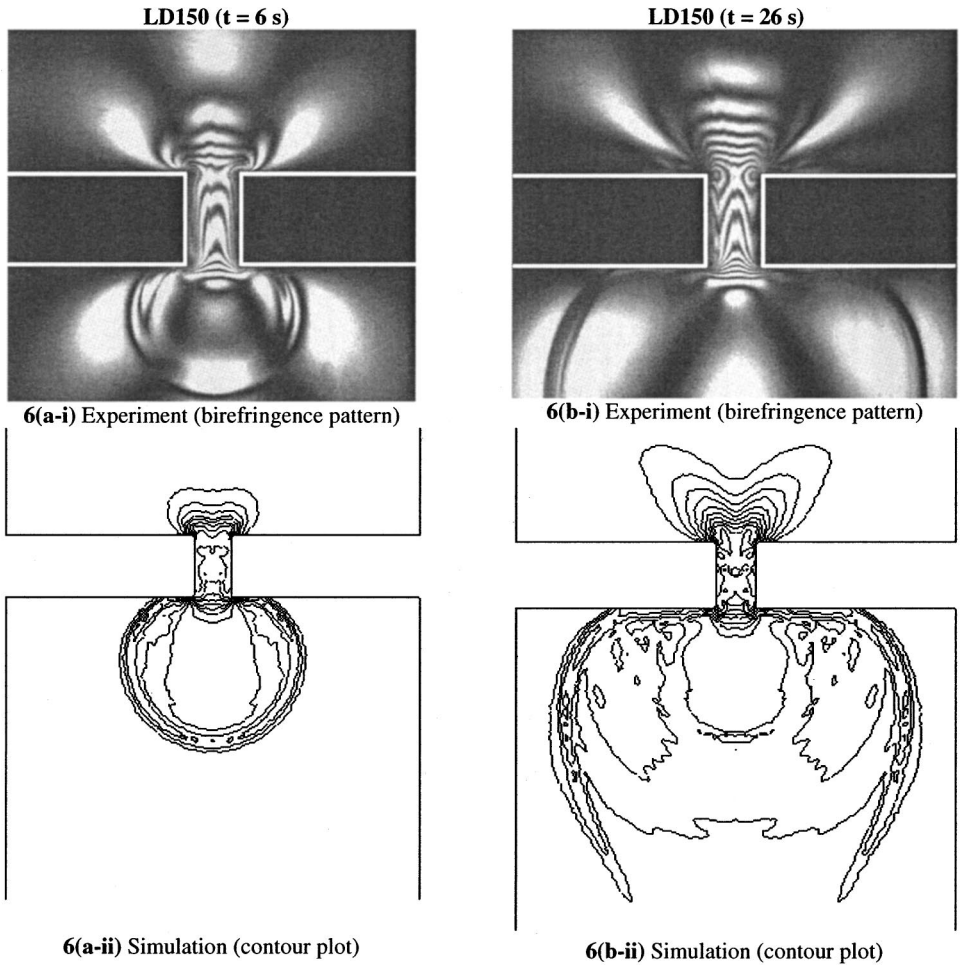

FIG. 6. Experimental flow birefringence pattern generated by a MPR, with the highest order retardation, k, at the symmetry axis and the entry region of the flow in (a-i) $k = 5$, at $t = 6$ s and (b-i) $k = 7$, at $t = 26$ s. The corresponding stress fields simulated in the flow solver at $t = 6$ s and 26 s, are given in (a-ii) and (b-ii), respectively. The step size of both contour plots of PSD is 6×10^4 Pa. The maximum level of simulated PSD in 6(b-ii) is 6×10^5 Pa.

Experimentally we observe, for LDPE, the time-dependant development of a localized region of stress concentration downstream of the contraction which we call ''transient stress fangs.'' The effect is striking and can clearly be seen in Fig. 6, both from experiments and from simulation. The stress fang emanates from material that has come from near the downstream throat of the slit. The second row, Figs. 6(a-ii) and 6(b-ii), show equally spaced contours of $\Delta\sigma$ for LDPE LD150 at two different times during the simulated start–up of flow, which should be compared with the experimental birefringence patterns (first row) in Figs. 6(a-i) and 6(b-i), respectively. Both sets of results clearly show the development of stress fangs. As time progresses, the stress fangs are ''pushed away'' from the central region of flow by material that has subsequently passed through the slit. The stress fang is thus seen to be a consequence of the start up deformation history, and not the steady flow condition. The stress increment used in Figs. 6(a-ii) and 6(b-ii) is 5.8×10^4 Pa whilst that observed in the multipass rheometer [using Eqs. (5) and

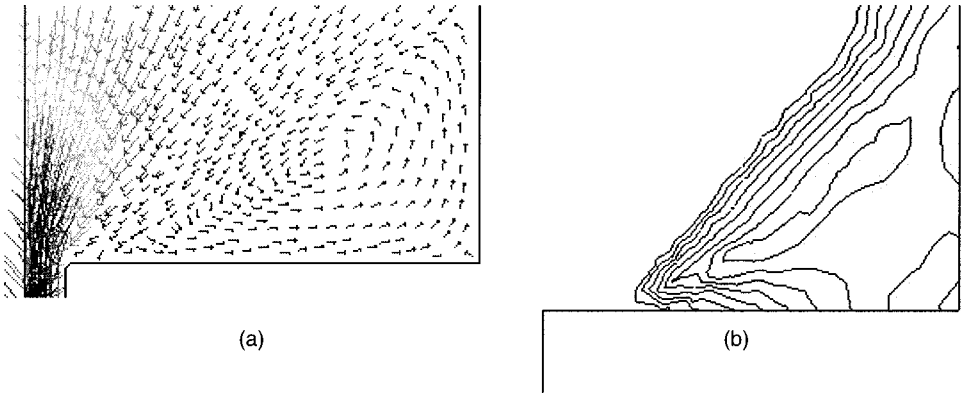

FIG. 7. Simulation results of (a) the upstream recirculation vortex (a vector plot of the velocity field) and (b) an enlargement of the PSD in this region with the maximum contour level set to one tenth of that in Fig. 6(b-ii), to illustrate the stress field near the vortex (flow is from top to bottom).

(6)] is 2.9×10^4 Pa. This difference is probably due to the three-dimensional effects that have not been captured by the simulation, however, by comparing both the density and shape of the simulated and experimental fringes in, and immediately outside, the constriction (where the flow has an effective 10:1 aspect ratio), we see that the simulations are near-quantitative.

Upstream of the die a recirculation vortex is visible both experimentally and numerically. Figure 7(a) shows the numerical prediction of this vortex at the same time as Figs. 6(b-i) and 6(b-ii) while Fig. 7(b) shows an enlargement of the $\Delta\sigma$ in this region with the maximum contour level set to one tenth that in Figs. 6(b-i) and 6(b-ii) to illustrate the stress field near the vortex. The numerical simulation appears to capture this feature qualitatively.

In contrast to the LDPE sample, a similar experimental/simulated start-up flow was carried out for the LLDPE DOWLEX and these results are shown in Fig. 8. These data

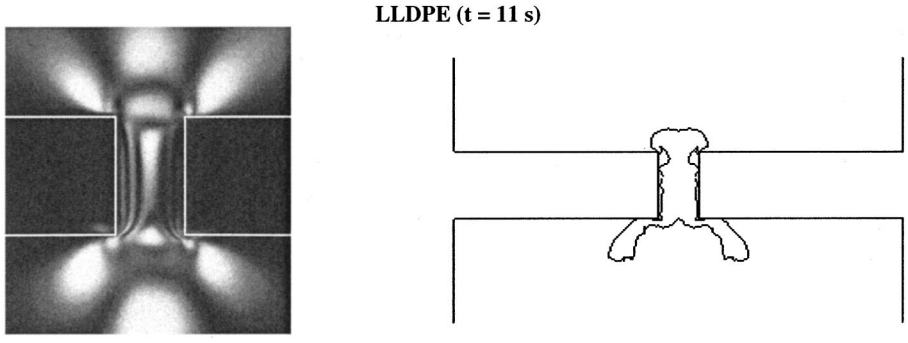

FIG. 8. (a-i) Experimental flow birefringence pattern in the MPR for LLDPE, with a highest order retardation at the symmetry axis and the entry region of the flow, $k = 1$; and (a-ii) the simulated stress field. The maximum level of simulated PSD for the LLDPE in 8(a-ii) is 8×10^4 Pa and thus only a single line is visible. Experimentally, at times 11 s and beyond (during start-up of flow), the fringe pattern obtained for the LLDPE appeared to reach a steady state.

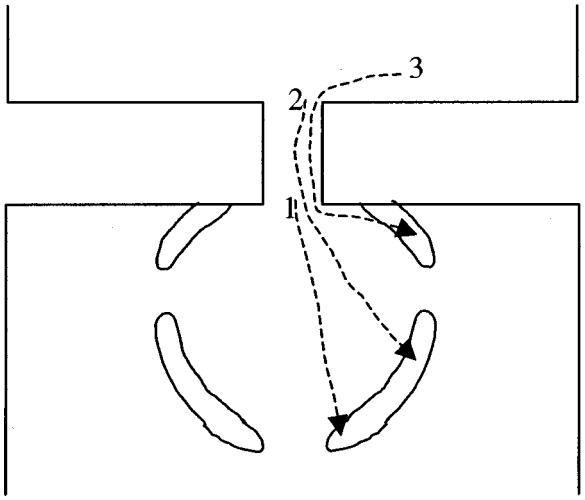

FIG. 9. A schematic that shows the tracking of triangle vertices during the first 7 s of the simulation for LD150.

show little evidence of any stress fang from either the experimental results or the numerical simulation. Here the maximum simulated PSD is 8×10^4 Pa (compared with 7×10^5 Pa for LD150) and thus, using the same stress increment as in Fig. 6, only a single line is observed. Better resolution upstream of the contraction could be seen by using a smaller value for the stress optical coefficient, however, it is unlikely that the experimental value is much different to that in the LDPE. Furthermore, a steady-state flow was observed with DOWLEX in approximately 12 s from the flow start-up, whereas, in the case of the LDPE LD150, we were unable to reach fully a steady-state condition, either experimentally or numerically.

The stress fang arises from the different strain history experienced by material that starts within the contraction from the material that follows it. Material that is initially upstream of the constriction experiences a contraction flow followed by an equal and opposite expansion flow, so that the net strain on the material is zero. However, material that is initially within the contraction only experiences the expansion flow and so receives a net strain. The expanding fang represents the position of this material as it is advected downstream. This is illustrated in Fig. 9 which shows the movement of three material points during the first 7 s of the simulation for LD150. Traces (1) and (2) show clearly that the material in the lower fang originates from the material that started in the constriction. Thus, the transient stress fang is seen as a remnant of the initial material in the constriction. Figure 10(a) shows the stretch in mode six at the same time as that in Fig. 6(a-ii). The stress fang corresponds to highly oriented material. The material that is most stretched is that which has been close to the wall of the slit, where the shear has oriented the pom–pom modes and thus allowed them to stretch more readily. A similar pattern is observed in all other modes that stretch (i.e., those with $q > 1$). For the other modes, the relative degree of stretch (λ/q, where q is the maximum stretch obtainable for the mode) is less; at the particular strain rate simulated, faster relaxing modes have time to relax whilst slower modes have larger values of q and will not be fully extended. The LLDPE [Fig. 10(b)] has quite a different structure of molecular stretch.

In Fig. 10 it can also be seen that upstream of the contraction the molecules are more highly stretched along the streamline coming from near the wall of the channel than from the center line where the extension rate is largest. A similar observation was made by

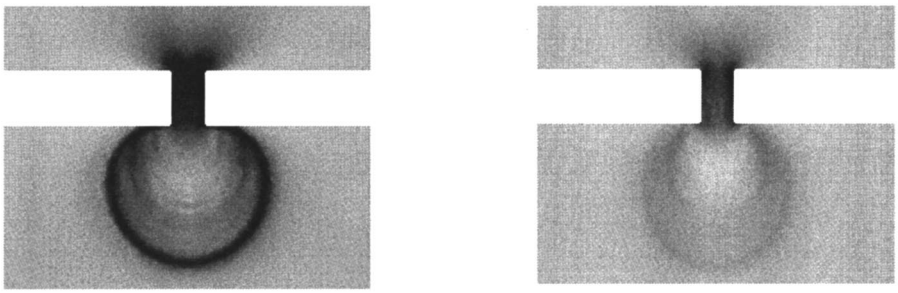

FIG. 10. (a) Stretch in the pom–pom mode six after 6 s. Black indicates the greatest pom–pom stretch, $\lambda = 4$. The flow is from top to bottom; (b) similar plot for the corresponding mode in the LLDPE.

Bishko *et al.* (1999). Material that starts near the wall experiences shear which tends to orient the backbones in the direction of flow. This preorientation makes the extensional flow more effective at stretching the molecules than for material along the center line that has not had this preshear.

The pressure difference across the flow cell in the MPR was measured as a function of time for both materials. The results for DOWLEX and LD150 are shown in Figs. 11(a) and 11(b). For the DOWLEX, at time 0 s, the pistons started to advance and following a rapid rise in ΔP, a steady pressure difference of approximately 3.0 bar was sustained for a total of 100 s. The approximate value of axial pressure difference, ΔP, of the frame in Fig. 9(a-i) (11 s after *start-up*) was $\sim$ 2.9 bar, as indicated by the filled symbol.

For the case of the LDPE LD150, a progressive increase in the pressure drop was observed during the observed experimental period. The approximate transient ΔPs corresponding to the frames $t = 6$ s and 26 s [Figs. 6(a-i) and 6(b-i)] was 6.6 and 7.8 bar, respectively. In Fig. 11(a), the ΔP increases gradually, reaching a pseudosteady state ($\Delta P \sim 8.3$ bar) and subsequently increasing marginally to reach a final value of approximately 9.6 bar. A similar transient response of the flow with the LD150 was also seen in terms of the evolution of its birefringence pattern.

The pressure drops observed in the simulated data are shown in Fig. 11(b). The results show a qualitatively similar pattern to the experimental data in that the pressure drop for the LLDPE DOWLEX reaches a plateau value very quickly, whilst that for the LD150 continues to rise slowly throughout the simulation. Note that quantitatively the prediction is better with the LLDPE. However, qualitatively the overall predicted transient profile of ΔP agrees well with the experimental ones for both PEs.

VI. DISCUSSION AND CONCLUSIONS

We have reported, for the first time, the appearance of transient stress fangs in a slit flow for a flowing molten polymer. The fangs appear to be a manifestation of the transient start-up history of the flow and both the rheology of the polymer and the shear history of the material influence their presence.

The MPR has been used as a precision extrusion device and it has been able to capture the effect for a particular slit geometry and LDPE. The rheology of the polymer is clearly important, as the effect was not seen for LLDPE. Compared to the entry flow, there has been relatively little attention paid to the exit flow from a slit into a reservoir. This flow is in fact more complex than the entry flow because the material can carry with it the memory of the upstream strain history.

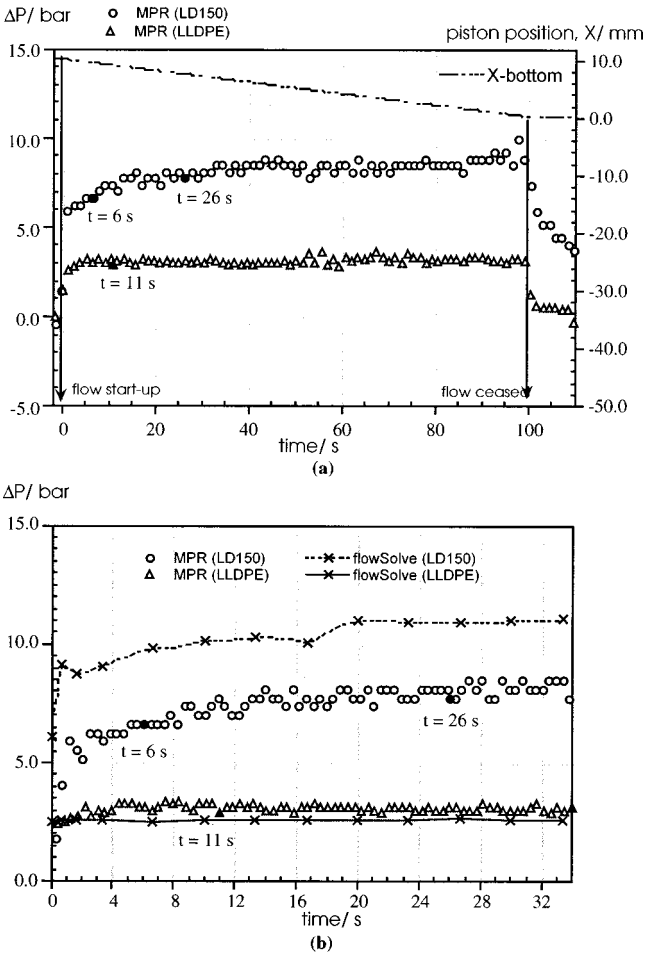

FIG. 11. Experimental and simulated overall transient pressure drop (ΔP) in the slit flow (apparent wall shear rate of 8.5 s^{-1}) (a) MPR profiles of ΔP (open symbols) and piston position (dashed line) during one single shot: piston speed, 0.1 mm s^{-1}; piston stroke, 5 mm; and idle time (between successive passes), 10 s. Closed symbols indicate measured DP for LLDPE at $t = 11$ s (s) and for LD150 at $t = 6$ s and 26 s (l), during start-up of flow. (b) Zoom of Fig. 11(a) showing the experimental (MPR) and simulated (flow solver) ΔP profiles during the first 34 s of flow start-up.

The multimode pom–pom constitutive equation that we have used, has been found to give a good fit to the rheological data available. The model combined with the numerical simulation also appears, qualitatively at least, to capture quite complex aspects of the flow. Both the time dependent stress field and pressure buildup show reasonable agreement with the experiment data and we believe that with further refinement of the numerical scheme, the match can be further improved. The time-dependent aspect of the simulation is crucial for the predictions of fangs and both the differential form of the constitutive equation and the Lagrangian tracking scheme used in this paper is well suited to this type of simulation. Representative wall shear rates for the experiments carried out in this paper are of the order of 10 s^{-1}. With maximum relaxation times of the order of 10^3 s, this means the maximum Weissenberg number for the flows are of the order of

10^4. This in turn indicates that the combined constitutive equation and simulation is able to handle challenging viscoelastic conditions.

Although the pom–pom model was initially conceived to describe branched polymers such as LDPE, it would appear from this work that it also has the potential to describe the flow behavior of essentially linear but polydisperse chains also.

ACKNOWLEDGMENTS

Financial support from the Commission of European Union through the BRITE-EURAM III ART Project No. (BE96-3490) is gratefully acknowledged together with EPSRC support from the Micro-scale Polymer Processing project. The authors would also like to thank Dow Chemicals and Dr. R. J. Koopmans for providing the extensional rheological data, and Dr. Bryan Crosby of Leeds University for fitting of the nonlinear parameters.

References

Ahmed, R., R. F. Liang, and M. R. Mackley, ''The experimental observation and numerical prediction of planar entry flow and die swell for molten polyethylene,'' J. Non-Newtonian Fluid Mech. **59**, 129–153 (1995).

Baaijens, F. P. T., ''Mixed finite element methods for viscoelastic flow analysis: A review,'' J. Non-Newtonian Fluid Mech. **79**, 361–385 (1998).

Baaijens, H. P. W., ''Evaluation of constitutive equations for polymer melts and solutions in complex flows,'' Ph.D. thesis, Eindhoven University of Technology, The Netherlands, 1994.

Baaijens, F. P. T., S. H. A. Selen, H. P. W. Baaijens, G. W. M. Peters, and H. E. H. Meijer, ''Viscoelastic flow past a confined cylinder of a low density polyethylene melt,'' J. Non-Newtonian Fluid Mech. **68**, 173–203 (1997).

Baaijens, F. P. T., W. M. H. Verbeeten, and G. W. M. Peters, ''Analysis of viscoelastic polymer melt flow,'' in Proc. of the XIIIth International Congress on Rheology, Cambridge, UK, 2000, Vol. 1, pp. 23–28.

Bernstein, B., E. A. Kearsley, and L. J. Zapas, ''A theory of stress relaxation with finite strain,'' Trans. Soc. Rheol. **7**, 391–410 (1963).

Bishko, G. B., O. G. Harlen, T. C. B. McLeish, and T. M. Nicholson, ''Numerical simulation of the transient flow of branched polymer melts through a planar contraction using the 'pom-pom' model,'' J. Non-Newtonian Fluid Mech. **82**, 255–273 (1999).

Blackwell, R. J., T. C. B. McLeish, and O. G. Harlen, ''Molecular drag-strain coupling in branched polymer melts,'' J. Rheol. **44**, 121–136 (2000).

Blackwell, R. J., O. G. Harlen, and T. C. B. McLeish, ''Theoretical linear and non-linear rheology of symmetric tree-like polymer melts'' Macromolecules (to be published).

Boger, D. V., M. J. Crochet, and R. A. Keiller, ''On viscoelastic flows through abrupt contractions,'' J. Non-Newtonian Fluid Mech. **44**, 267–279 (1992).

Davies, A. R. and J. Devlin, ''On corner flows of Oldroyd B fluids,'' J. Non-Newtonian Fluid Mech. **50**, 173–191 (1993).

Doi, M. and S. F. Edwards, *The Theory of Polymer Dynamics* (Oxford University Press, New York, 1996).

Harlen, O. G., J. M. Rallison, and P. Szabo, ''A split Lagrangian-Eulerian method for simulating transient viscoelastic flows,'' J. Non-Newtonian Fluid Mech. **60**, 81–104 (1995).

Hinch, E. J., ''Flow of an Oldroyd B fluid round a sharp corner,'' J. Non-Newtonian Fluid Mech. **50**, 161–171 (1993).

Inkson, N. J., T. C. B. McLeish, O. G. Harlen, and D. J. Groves, ''Predicting low density polyethylene melt rheology in elongational and shear flows with ''pom-pom'' constitutive equations,'' J. Rheol. **43**, 873–896 (1999).

Kiriakidis, D. G., H. J. Park, E. Mitsoulis, B. Vergnes, and J.-F. Agassant, ''A study of stress distribution in contraction flows of an LLDPE melt,'' J. Non-Newtonian Fluid Mech. **47**, 339–356 (1993).

Koopmans, R. J., ''Extrudate swell of high density polyethylene, part I: Aspects of molecular structure and rheological characterization methods; Part II: Time dependency and effects of cooling and sagging,'' Polym. Eng. Sci. **32**, 1741–1749 (1992).

Lee, K. and M. R. Mackley, ''The significance of slip in matching polyethylene processing data with numerical simulation,'' J. Non-Newtonian Fluid Mech. **94**, 159–177 (2000).

Mackley, M. R. and P. H. J. Spitteler, "Experimental observations on the pressure-dependent polymer melt rheology of linear low density polyethylene using a multi-pass rheometer," Rheol. Acta **35**, 202–209 (1996).

Mackley, M. R., R. T. J. Marshall, and J. B. A. F. Smeulders, "The multipass rheometer," J. Rheol. **39**, 1293–1309 (1995).

Mackley, M. R., R. T. J. Marshall, J. B. A. F. Smeulders, and F. D. Zhao, "The rheological characterisation of polymeric and colloidal fluids," Chem. Eng. Sci. **49**, 2551–2565 (1994).

McLeish, T. C. B. and R. G. Larson, "Molecular constitutive equations for a class of branched polymers: The pom-pom polymer," J. Rheol. **42**, 81–110 (1998).

Osaki, K., S. Kimura, M. Kimura, and M. Kurata, "Relaxation of shear and normal stresses in double-step shear deformation for a polystyrene solution-A test of the Doi–Edwards theory for polymer rheology," J. Rheol. **25**, 548–562 (1981).

Phan-Thien, N. and R. I. Tanner, "A new constitutive equation derived from network theory," J. Non-Newtonian Fluid Mech. **2**, 353–365 (1977).

Phan-Thien, N., "A nonlinear network viscoelastic model," J. Rheol. **22**, 259–283 (1978).

Ranganathan, M., M. R. Mackley, and P. H. J. Spitteler, "The transient rheology and processing of polyethylene melts," J. Rheol. **43**, 443–451 (1999).

Renardy, M., "A matched solution for corner flow of an upper convected Maxwell fluid," J. Non-Newtonian Fluid Mech. **50**, 83–89 (1993).

Rutgers, R. P. G., "An experimental and numerical study of extrusion surface instabilities for polyethylene melts," Ph.D. thesis, Department of Chemical Engineering, University of Cambridge, Cambridge, UK, 1998.

Tanner, R. I., "Some useful constitutive models with a kinematic slip hypothesis," J. Non-Newtonian Fluid Mech. **5**, 103–112 (1979).

Wagner, M. H. and P. Ehrecke, "Dynamics of polymer melts in reversing shear flows," J. Non-Newtonian Fluid Mech. **76**, 183–197 (1998).

Wagner, M. H. and H. M. Laun, "Non-linear shear creep and constrained elastic recovery of a LDPE melt," Rheol. Acta **17**, 138–148 (1978).

Wales, J. L. S., "The application of flow birefringence to rheological studies of polymer melts," Ph.D. thesis, Technische Hogeschool Delft, The Netherlands, 1976.

White, S. A., A. D. Gotsis, and D. G. Baird, "Review of the entry flow problem: Experimental and numerical," J. Non-Newtonian Fluid Mech. **24**, 121–160 (1987).